Journal of Engineering Mathematics (2024) 146:2
https://doi.org/10.1007/s10665-024-10352-4

Droplet impact onto a porous substrate: a Wagner theory for early-stage spreading

Gavin Moreton[1,2] · **Richard Purvis**[1] · **Mark J. Cooker**[1]

Received: 4 October 2023 / Accepted: 26 February 2024

Abstract
An analytical model for droplet impact onto a porous substrate is presented, based on Wagner theory. An idealised substrate boundary condition is introduced, mimicking the effect of fluid entry into a genuinely porous substrate. The asymptotic analysis yields a solution for a small porous correction with free-surfaces and pressures compared with the impermeable case. On a global scale, it is found that the impact region on the substrate grows more slowly with porosity included due to loss of mass into the substrate. The spatial distribution of liquid volume flux into the substrate is also described. Locally near the turn-over regions, the expected jetting along the surface is calculated with the same volume flux but the jet is found to be slower and thicker than for an impermeable substrate.

Keywords Asymptotics · Droplet impact · Porous substrate · Splashing · Splashing/jetting · Wagner theory

1 Introduction

Droplet impacts onto porous surfaces form a key part of many processes, ranging from the control of accurate ink-jet printing [1–3], to the erosion of porous soils [4, 5], the penetration or removal of liquid contaminent ingress into concrete [6] and spreading on

✉ Richard Purvis
r.purvis@uea.ac.uk

Gavin Moreton
gtm2@leicester.ac.uk

Mark J. Cooker
m.cooker@uea.ac.uk

[1] School of Mathematics, University of East Anglia, Norwich Research Park, Norwich NR4 7TJ, UK

[2] School of Computing and Mathematical Sciences, University of Leicester, University Road, Leicester LE1 7RH, UK

Published online: 17 April 2024

natural porous stone [7]. Experimental droplet impact studies have shown that porous substrates can significantly reduce splashing during impact [8–10]. Complex substrates designed with micro-pillars have been engineered, recreating the repellant properties of lotus leaves [11, 12], and shown to have hydrophobic properties potentially suitable for preventing icing on aircraft during flight through clouds [13, 14]. Micro-structured surfaces are increasingly used to control liquid behaviour by introducing hydrophobic or hydrophillic properties [15–17], and while such surface effects can be retained with low-speed impacts, the behaviour for higher-speed impacts when water can penetrate significantly into the substrate is still not fully understood. Across these applications, it is evident that violent impacts onto both saturated and unsaturated porous media are important. A fuller insight into impacts onto porous surfaces will allow further design progress towards controlling impacts, either supressing splashing completely or enhancing ejection of material from the surface, depending on the application.

Droplet impacts onto solids and subsequent splashing have been widely studied experimentally, analytically and numerically; thorough reviews of the area have been provided by [18–20]. The main theoretical approach to modelling liquid–solid impacts is the standard Wagner model of post impact dynamics which was originally developed to predict pressures on landing aircraft [21]. It uses inviscid potential flow to study the entry of a solid body into a water layer, coupled with the Wagner condition that the liquid free-surface meets the solid body at turnover points at the edge of a wetted region. This approach was subsequently applied to ship slamming [22, 23], and the asymptotic structure was shown to formally hold by Oliver [24]. On the largest outer scale, a boundary value problem is obtained subject to mixed boundary conditions where the transition points between the wetted and dry parts of the solid are unknown in advance. Singular pressures are found at these turnover points, and each of these is resolved by a local jet-root region which predicts the formation of a fast moving splash jet. The same theoretical framework extends to modelling droplet impacts. Past investigations have included droplet impacts onto thin liquid layers [25], onto flat substrates with isolated roughness [26], onto non-flat surfaces [27], onto elastic substrates [28, 29] and freezing during supercooled droplet impacts onto ice [30]. However, little investigation has been reported for Wagner impact onto porous substrates, although there has been study of the penetration into a porous surface by impacting fluid [31–33] in other regimes.

This current work looks to extend Wagner theory to include the presence of a porous substrate (see also [34]). As a first step towards a fully-coupled description combining the inertial Wagner approach with (for example) a Darcy flow in a porous substrate, the current work adopts an imposed boundary condition on the substrate intended to closely mimic a full porous model. In particular, our desire is to both understand how flow into the substrate affects the overall splashing behaviour, and understand if the asymptotic structure of the Wagner solution is maintained for porous substrates. Section 2 below outlines our approach in detail, before the full resulting analytical problem is derived and solved. Results and a detailed discussion of the influence of porosity on the splash jets are provided.

2 Modelling approach and overview

In this section we describe the strategy for the rest of the paper. Our aim here is to describe the physical setting from which we derive our mathematical model. To establish our theory, we first carry out scalings to identify dimensionless small-valued parameters in the problem. The first small parameter, ϵ, underlies Wagner theory of liquid impact [24]. Its small value comes from the brief time of impact being small compared with the longer time R/V, where R is the size of the droplet and V is the closing speed just before impact. Secondly, the principal parameter of our analysis for flow into a porous substrate is k. If $k = 0$, then this corresponds to impermeable substrate—a special case which we solve first in Sect. 3.2. The results of Sect. 3.2 are used to inform the subsequent asymptotic analysis for small positive k, in Sect. 3.1. (In the course of the asymptotic analysis at first order in k, we neglect terms of size $O(k^2)$ because they are relatively small compared with retained terms of size $O(k)$.)

At the start of this study the authors wanted to answer the following questions about how porosity influences the flow: How much of the droplet fluid can enter the substrate under the brief and high-pressure conditions of a sudden impact? Does the substrate slow down or speed up the spreading of the impact region? In the impact region, is the pressure reduced or increased by porosity? What happens to the splash jet: is it thicker or thinner? In this work these qualitative questions are answered quantitatively, and we hope our theoretical results will bear comparison with future experimental measurements.

We neglect surface tension because impact pressures greatly exceed the magnitude of the capillary-pressure jump across a droplet's free surface. We neglect air effect here, further discussion of pre-impact air-cushioning effects including porosity can be found in [34, 35]. We justify setting $p = 0$ on the free-surface here as the inertia of the air is small compared with that of the water [36]. We can justify an inviscid fluid model as the Reynolds number, Re, is large. For a water drop of kinematic viscosity $\nu = 10^{-6}\,\mathrm{m}^2/\mathrm{s}$, an impact speed $V = 10\,\mathrm{m/s}$, and a droplet radius $R = 10^{-3}\,\mathrm{m}$, we have the Reynolds number $Re = VR/\nu \sim 10^4$, the Weber number $We = \rho V^2 R/\sigma \sim 10^3$ and the Froude number $Fr = U/\sqrt{gR} \sim 10^2$. The large values of We and Fr allow us to neglect capillarity and gravity, respectively.

We treat the flow as a two-dimensional, left-right symmetric, incompressible fluid in irrotational flow. The y^* axis points vertically up, where starred variables are at physical scale in Sect. 3. Figure 1 shows the curved surface of the drop meeting the horizontal top of the substrate in a contact region which is a finite interval of the x^* axis. The contact interval, $-d^*(t^*) \le x^* \le d^*(t^*)$, lies between the two turnover points, at $x^* = \pm d^*(t)$. A turnover point is so called because on the right side of the drop the free surface turns around a tight bend, or turnover, to join a thin jet that flows along the positive x^* axis. In Wagner theory the jet has negligible $O(\epsilon^2)$ thickness, so that at $O(\epsilon)$ the drop's free surface is supposed to meet the solid surface at $y^* = 0$, with negligible error in position. We return to model the consequent flow in the jet-root region and the changes to it due to porosity, in Sect. 5.

Returning to the impact region, the important function $d^*(t^*)$ increases monotonically from zero at the instant of initial contact, $t^* = 0$, as the fluid spreads over the substrate. Since the curved droplet is locally of parabolic initial shape, Wagner theory

tells us that d^* increases proportional to $\sqrt{t^*}$. The impact region spreads fast at early times and later slows down. Understanding the dependences of d^* on time and on porosity k are important for all our analysis. The free-boundary problem that we solve depends sensitively on a precise description of d^*, as it defines the central region of contact and the innermost points of the drop's free surface. The fact that d^* depends on k means that the $O(k)$ problem is posed with a *different impact region* from the $k = 0$ impermeable case. We find that every part of the solution depends on d^* via integral expressions, with $\pm d^*$ the limits of integration, and where the integrands have singularities at these end points. It has been a job of work for the authors to show how the results depend on d^*, and to find the correct form of expansion of d^* as a function of k, in order to reach mathematically consistent results. This is not a classical asymptotic analysis. One of our strategies has been to retain d^* as a general quantity until as late as possible in the analysis, delaying expressing it until we show it must have a particular form to keep the model equations consistent.

Wagner theory allows us to linearise the equations and throw the boundary conditions onto the x^* axis (even in the presence of porosity). The fluid domain is then approximated by the upper half-plane, in which Laplace's equation is the governing relation for the drop's fluid in irrotational flow. See Fig.2. The importance of d^* is central because we must impose different types of boundary condition in the impact zone $[-d^*, d^*]$ from that on the sections of free surface $(-\infty, -d^*]$ and $[d^*, \infty)$. Mathematically, the model is a mixed boundary value problem. Physically, the boundary conditions come from distinct constraints on the flow: the liquid must have zero pressure on the segments of free surface, whereas in the impact region the normal velocity component is either zero ($k = 0$, impermeable) or modified by the porous substrate ($k > 0$, permeable) at the solid–liquid boundary. In Sect. 3.2 we derive a condition on the normal derivative of the velocity potential which accommodates the idea of fluid being forced into the substrate by the high-pressure impacting liquid.

In the next section we lay out our model equations for a theory up to $O(k)$. In Sect. 3.2 we solve the special impermeable case ($k = 0$), following classical Wagner theory. In Sect. 3.1 we address the $O(k)$ problem, with help from the results of Sect. 3.2. The results are presented in Sect. 4.

3 Wagner problem for impact onto a porous substrate

3.1 Governing equations

We now consider a droplet impact with a flat-topped substrate in two dimensions. The starred variables are physical and have S.I. units, and we rescale them below. We choose for simplicity a stationary droplet, with radius R, and the substrate rising at velocity V; the substrate's top is at $y^* = 0$ at the time of initial impact $t^* = 0$. After impact starts at $t^* = 0^+$, Wagner Theory is used to describe the impact behaviour; see Fig. 1 for details and a schematic of the flow structure. The y^* axis increases vertically up into the fluid with $x^* = 0$ being a line of symmetry for the problem. The liquid free-surface is given by $y^* = \eta^*(x^*, t^*)$, but we are only interested in the impact region, the lowest part of the droplet. The free surface deforms from the start

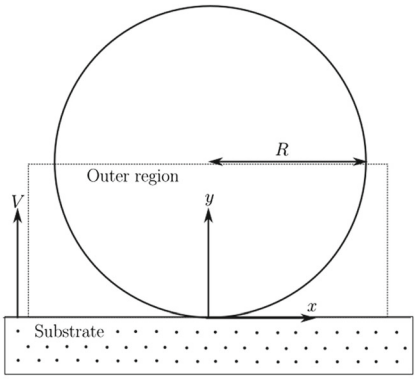

(a) Diagram showing the basic scales at $t^* = 0$.

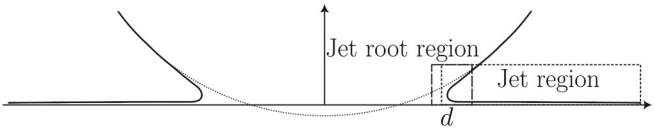

(b) Diagram showing the multiple regions of the problem near the right-hand turnover point.

Fig. 1 Diagrams showing **a** the initial situation, and **b** a schematic of the different asymptotic regions. In **b** the outer region has horizontal and vertical length scales of ϵ by ϵ. The asymptotically smaller jet root inner region has length scales of ϵ^2 by ϵ^2, and the long and thin jet retains the ϵ^2 vertical length scale

of impact onwards in time, and the substrate has a wetted region and a dry region as the droplet spreads after impact. On $y^* = Vt$, the interval $-d^*(t) \leq x \leq d^*(t)$ describes the region of impact of the liquid and the substrate. On the right half of the symmetric domain $x^* = d^*(t)$ is a turnover point at the root of a splash jet. Within the $O(\epsilon)$ Wagner asymptotics the turnover point is so close to the substrate that it is placed on the surface of the substrate, and the small height of the splash $(O(\epsilon^2))$is neglected (see also [24, 36]). The turnover points are symmetrically arranged on the plate at $x^* = \pm d^*(t)$ on $y^* = t^*V$ (due to the plate moving vertically) where $d^*(t)$ increases from $d^* = 0$ at $t^* = 0$, as time progresses. We expect if the drop is initially stationary then the disturbance of the free surface tends to zero as we pass into the far field.

Figure 1 shows the basic scales and geometry of the problem, and provides a schematic for the different local regions. The Wagner analysis that follows splits into three-distinct parts. Firstly, we consider the outer problem which considers the shape of the free surface. In this region the horizontal and vertical length scales are both $O(\epsilon)$, the lower droplet free-surface linearises onto $y = 0$, and the thin splash jets and turn-over regions are negligible on this scale. Secondly, at a more local view, we have the jet-root region (which is of size $O(\epsilon^2)$ by $O(\epsilon^2)$) and is where the free-surface turns over and forms the base of the jet which resolves the singularities found in the outer solution. Thirdly, this then ejects fluid into a long jet region, where we have a very thin jet running along the surface of the substrate.

Our governing equations for the outer problem are:

$$\nabla^2\phi^*(x^*, y^*, t^*) = 0 \quad \text{in fluid domain} y^* > \eta^*, \tag{1}$$

$$\frac{D}{Dt^*}(y^* - \eta^*) = 0 \quad \text{on } y^* = \eta^*(x^*, t^*) \text{ from the kinematic condition,} \tag{2}$$

$$p^*(x^*, y^*, t^*) = 0 \quad \text{on } y^* = \eta^* \text{ from zero stress on the free-surface,} \tag{3}$$

$$\frac{\partial\phi^*}{\partial y^*} = v^* \quad \text{on the plate } y^* = Vt^* \text{ when } |x^*| < d(t^*), \tag{4}$$

where D/Dt is the material derivative. In (4), we introduce a general substrate velocity $v^*(x^*, y^*, t^*, k^*, p_l^*, p_s^*)$ to enable inclusion of porous effects into the Wagner model, where k^* is a measure of the permeability of the substrate and where p_l^* and p_s^* correspond to pressures in the liquid and substrate, respectively. For the standard Wagner impact of a droplet with an impermeable substrate, we have simply a zero penetration condition $v^* = V$ (see below).

For initial conditions, we have an undisturbed lower portion of the circular droplet given by

$$\eta^*(x^*, 0) = R - \left(R^2 - x^{*2}\right)^{\frac{1}{2}} \tag{5}$$

or

$$\eta^*(x^*, 0) = \frac{x^{*2}}{2R} + O\left(\frac{x^{*4}}{2R^3}\right), \tag{6}$$

which is a form we use later for matching the initial conditions in the far-field.

We non-dimensionalise by scaling spatial coordinates with R, taking our velocity scale to be V, and hence a time scale of $\frac{R}{V}$. The free-surface shape is scaled in the same way as our spatial coordinates, ρV^2 gives the appropriate inviscid pressure scale (where ρ is the constant density of the fluid) and we scale velocity potential as RV. Thus we define new barred variables in terms of the physical variables by

$$[x^*, y^*, t^*, \phi^*, \eta^*, p^*, v^*] = \left[R\bar{x}, R\bar{y}, \frac{R}{V}\bar{t}, RV\bar{\phi}, R\bar{\eta}, \rho V^2\bar{p}, V\bar{v}\right]. \tag{7}$$

Hence our problem becomes in nondimensional terms

$$\nabla^2\bar{\phi}(\bar{x}, \bar{y}, \bar{t}) = 0 \quad \text{in fluid domain } \bar{y} > \bar{\eta}, \tag{8}$$

$$\frac{D}{D\bar{t}}(\bar{y} - \bar{\eta}) = 0 \quad \text{on } \bar{y} = \bar{\eta}(\bar{x}, \bar{t}), \tag{9}$$

$$\bar{p} = 0 \quad \text{on } \bar{y} = \bar{\eta}(\bar{x}, \bar{t}) \tag{10}$$

$$\frac{\partial\bar{\phi}}{\partial\bar{y}} = \bar{v} \quad \text{on plate, } \bar{y} = \bar{t} \text{ and } |\bar{x}| < d(\bar{t}). \tag{11}$$

We make further simplifications by considering only small times after impact, and focussing on the outer region sketched in Fig. 1. In particular, and in keeping with Wagner theory, we rescale and define new (undecorated) variables by

$$[\bar{x}, \bar{y}, \bar{t}, \bar{\phi}, \bar{\eta}, \bar{p}] = \left[\epsilon x, \epsilon y, \epsilon^2 t, \epsilon\phi, \epsilon^2\eta, \epsilon^{-1} p\right], \tag{12}$$

where ϵ is a small parameter, associated with the small slope of the liquid free surface near the turnover points in this outer solution. With the plate rising into the droplet the displacement of each turnover point is proportional to $\sqrt{t} \sim O(\epsilon)$ (originally observed by Wagner [21], and formalised mathematically by [24]), therefore the horizontal length scale is $O(\epsilon R)$, and is comparable via the continuity equation to the vertical scale of the region of influence of impact. The pressure scale follows from Bernoulli's equation.

For convenience we define a function $h(x, t)$ which is the perturbation from the initial shape of the droplet, so the position of the free surface is

$$\eta(x, t) = \frac{x^2}{2} - h(x, t). \tag{13}$$

Since $\eta \sim x^2/2$ from (6) as $x \to \infty$, this gives desirable behaviour as $h(x, t) \to 0$ as $|x| \to \infty$.

Applying the scales (12) to the boundary conditions, the free-surface conditions linearise to be evaluated on $y = 0$, and our problem reduces to the following mixed boundary value problem in the upper half plane:

$$\nabla^2\phi(x, y, t) = 0 \qquad \text{in the droplet } y > 0, \tag{14}$$

$$\frac{\partial\phi(x, 0, t)}{\partial y} = v(x, t) \qquad \text{on } |x| < d, \tag{15}$$

$$\phi(x, 0, t) = 0 \qquad \text{on } |x| > d. \tag{16}$$

We note that from the linearised Bernouilli equation, the liquid pressure in the impact zone can be found from

$$p(x, 0, t) = -\phi_t(x, 0, t) \qquad \text{for} \qquad |x| < d(t).$$

The time integral of this relation on the free surface where $p = 0$ supplies the boundary condition (16). We also require this for the boundary condition in the impact zone when the substrate is porous. The free-surface and far-field conditions are

$$\frac{\partial\phi(x, 0, t)}{\partial y} = \frac{\partial\eta(x, t)}{\partial t} \qquad \text{on } |x| > d, \tag{17}$$

$$\eta(x, t) \to \frac{x^2}{2} \qquad \text{as } |x| \to \infty, \tag{18}$$

$$\phi \to 0 \qquad \text{as } y \to \infty, \tag{19}$$

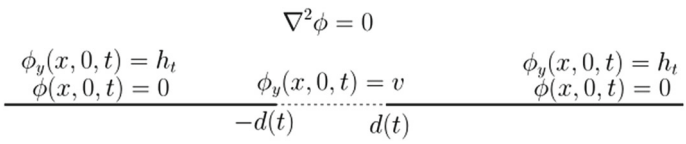

Fig. 2 Summary of the boundary conditions for the dimensionless problem

$$\phi(x,0,t) = 0 \qquad \text{on } |x| > d, \tag{20}$$

where $\phi(x, y, t)$, $\eta(x, t)$ and $d(t)$ are all unknown functions with $v(x, t)$ in (15) changing depending on the substrate. For the standard Wagner impact problem with an impermeable substrate $v = 1$ here; we present an alternative relation for $v(x, t)$ below to model the case when the substrate is porous.

On the scales of the outer problem described here, Wagner theory determines the position of the unknown turnover points $d(t)$ by ensuring that the free-surface height at the turnover points matches the vertical position of the plate. At $O(\epsilon)$ this is

$$\eta(d(t), t) - t = \frac{d(t)^2}{2} - h(d(t), t) - t = 0, \tag{21}$$

where $y = \eta(d(t), t)$ is the free-surface position and $y = \epsilon t$ is the position of the plate.

As discussed above, our focus in the current paper is to investigate how porosity of the substrate can be incorporated into Wagner theory. As a first step towards a full coupling of (for example) Darcy flow in a porous substrate with potential flow in the droplet, we introduce here a simplified model for the contribution to ϕ_y on the boundary between the droplet and the supposed porous substrate. The impermeable case forces us to include the condition that the normal velocity component (in the droplet's frame of reference) is $\phi_y = 1$. When the boundary is permeable ($k > 0$), we expect a change directly proportional to both k and the pressure driving the fluid into the substrate. In view of Darcy's law we do not know the normal component of the *gradient* in pressure but we do expect it to be proportional to the pressure at the top boundary of the substrate. Another consideration is that the liquid pressure $p(x, 0, t)$ is mildly singular at $x = \pm d$ and singular in time at $t = 0$. In order to keep the forcing finite within the impact interval, we include another factor d. We recognise that the product of $d(t)$ and p_l is the substrate's upward force on the drop that brings about a change in momentum in the droplet. Putting these factors together we have

$$\phi_y = 1 - kd(t)p(x, 0, t). \tag{22}$$

The minus sign is chosen to ensure that a positive liquid pressure corresponds to fluid penetrating the substrate. From the linearised version of Bernoulli's equation we also have $p = -\phi_t$. Hence we impose

$$\phi_y = 1 + kd(t)\phi_t(x, 0, t). \tag{23}$$

Note that in (22) and (23) we are not specifying any details of the flow inside the porous layer, including pre-saturation or the subsequent flow in the substrate. We assume the substrate is essentially passive and just admits droplet fluid without reference to the local flow within the porous medium. If saturated, we'd expect either a substrate-bed infuence or displacement of fluid from the substrate up into the drop. If unsaturated, we'd expect the droplet fluid to just penetrate a short distance (compared with $d(t)$) into the substrate. In that sense, our model likely more closely resembles an unsaturated substrate.

We also need to relate k to physical constants. Rescaling back to the physical variables the dimensionless constant $k = CV/R$, where the porosity, C, is a material constant with dimensions of time. (Constant C is the same as that present in Darcy's law when expressing the fluid velocity in the substrate as: $\mathbf{v} = -C\rho^{-1}\nabla p$.) We are interested in a regime in which $k = CV/R$ is small. For example, a depth of fluid penetration, CV, much less than the droplet radius R. (The previous scaling by powers of ϵ affects neither the definition of k nor the discussion of k as a ratio of distinct physical times, or physical fluid speeds.) We are extending the substrate condition used in Hicks et al. [6] where a constant penetration velocity was assumed across a wetted region based on a centreline pressure at $x = 0$.

Although strictly we could impose (23) as an approximation for any k, we restrict ourselves here to the case of small porosity and assume that $k \ll 1$. Of course, a full realistic condition would require resolving a fully coupled Darcy problem in the substrate. The current work looks to investigate how such porous effects might be incorporated into the framework of the Wagner solution as a first step towards understanding the full problem. Given our assumption of small k, we look to develop an asymptotic solution. Hence, assuming a regular asymptotic expansion in powers of the small parameter k exists, we expand the unknown functions as

$$\phi(x, y, t) = \phi_I(x, y, t) + k\phi_p(x, y, t) + O(k^2), \tag{24}$$

$$h(x, t) = h_I(x, t) + kh_p(x, t) + O(k^2), \tag{25}$$

$$d(t) = d_I(t) + kd_p(t) + O(k^2), \tag{26}$$

where subscripts I and p mark inpermeable and porous, respectively. Note that, in the analysis that follows, we find that for mathematical balance the correct expansion for the contact points is in the form

$$d_I(t) = 2t^{\frac{1}{2}} \qquad \text{and} \qquad d(t) = d_I(t) + kat^{\frac{1}{2}}, \tag{27}$$

for some constant a. Our problem now decouples into a leading order problem that excludes porosity (and is the standard Wagner problem for droplet impact onto an impermeable base), and a correction at $O(k)$ that will provide the initial changes to the flow due to flow into the substrate. A difficulty is that the size of the contact region defines the limits on integral expressions for the unknowns. We persist with our analysis using the general form of $d(t)$ until as late as possible before expanding it as (27), otherwise the integrals become unmanageable.

3.2 Leading order Wagner solution

For completeness, and as we need these results later in the porous correction Sect. 3.3, we present here the $k = 0$ solution for ϕ_I, h_I and the unknown turnover points d_I. We look to solve the system (14)–(21), with $v = 1$. The mixed boundary value problem we have for $\phi_I(x, y, t)$ is harmonic and together with the stream function $\psi_I(x, y, t)$ this pair of functions satisfy the Cauchy–Riemann equations. Letting $z = x + iy$, and defining on the real axis and in the upper half plane D, the characteristic function

$$\Delta(z) = \sqrt{z^2 - d_I^2},$$

we introduce a complex-valued function which is analytic on the real axis and in the upper half plane D,

$$w(z, t) = \Delta(z)(\phi_I(x, y, t) + i\psi_I(x, y, t)). \tag{28}$$

The presence of the factor $\Delta(z)$ regularizes singular behaviour in the complex velocity potential. Using Cauchy's integral formula in principal value form for w, for z inside D, we obtain

$$\phi_{I,x} - i\phi_{I,y} = \frac{1}{2i\pi\,\Delta(z)} \oint_\Gamma \frac{\Delta(\gamma)(\phi_{I,\alpha}(\alpha, \beta, t) - i\phi_{I,\beta}(\alpha, \beta, t))}{\gamma - z} \mathrm{d}\gamma, \tag{29}$$

with $\gamma = \alpha + i\beta$, and where the Cauchy–Riemann equations have been used to eliminate ψ_I. Taking real and imaginary parts, and evaluating over a simple closed contour Γ in the upper half plane running along $y = 0$ and then returning anticlockwise through a semicircular arc through the droplet, and allowing for the singular behaviour on $\beta = 0$ at $\alpha = x$, (29) becomes the pair of relations:

$$\begin{aligned}\phi_{I,x}(x, 0, t) = \frac{1}{\pi\sqrt{d_I^2 - x^2}} \Bigg[&\int_{d_I}^{\infty} \frac{\sqrt{\alpha^2 - d_I^2}\phi_{I,\alpha}}{\alpha - x} \mathrm{d}\alpha \\ &+ P.V. \int_{-d_I}^{d_I} \frac{\sqrt{d_I^2 - \alpha^2}\phi_{I,\beta}}{\alpha - x} \mathrm{d}\alpha + \int_{-\infty}^{-d_I} \frac{\sqrt{\alpha^2 - d_I^2}\phi_{I,\alpha}}{\alpha - x} \mathrm{d}\alpha \Bigg]\end{aligned} \tag{30}$$

for $|x| < d_I(t)$, and

$$\begin{aligned}-\phi_{I,y}(x, 0, t) = \frac{1}{\pi\sqrt{x^2 - d_I^2}} \Bigg[&P.V. \int_{d_I}^{\infty} \frac{\sqrt{\alpha^2 - d_I^2}\phi_{I,\alpha}}{\alpha - x} \mathrm{d}\alpha \\ &+ \int_{-d_I}^{d_I} \frac{\sqrt{d_I^2 - \alpha^2}v}{\alpha - x} \mathrm{d}\alpha + P.V. \int_{-\infty}^{-d_I} \frac{\sqrt{\alpha^2 - d_I^2}\phi_{I,\alpha}}{\alpha - x} \mathrm{d}\alpha \Bigg]\end{aligned} \tag{31}$$

for $|x| > d_I(t)$. The letter $P.V.$ denote the principal-value. These relations simplify by imposing boundary conditions (15)–(17) becoming

$$\phi_{I,x}(x,0,t) = \frac{1}{\pi\sqrt{d_I^2 - x^2}} P.V. \int_{-d_I}^{d_I} \frac{\sqrt{d_I^2 - \alpha^2}}{\alpha - x} \mathrm{d}\alpha \qquad \text{for } |x| < d_I(t) \tag{32}$$

and

$$-\phi_{I,y}(x,0,t) = -\eta_t = h_{I,t} = \frac{1}{\pi\sqrt{x^2 - d_I^2}} \int_{-d_I}^{d_I} \frac{\sqrt{d_I^2 - \alpha^2}}{\alpha - x} \mathrm{d}\alpha \qquad \text{for } |x| > d_I(t) \tag{33}$$

where we are imposing $v = 1$, for the moment. Evaluating the integral in (33) yields

$$h_{I,t} = -1 + \frac{x}{\sqrt{x^2 - d_I^2}}, \tag{34}$$

agreeing with the results in Oliver [24]. Integrating (34) with respect to time, and assuming the initial droplet is undisturbed in the far-field (18), we find

$$h_I(x,t) = -t + \int_0^t \frac{x}{\sqrt{x^2 - d_I(\tau)^2}} \mathrm{d}\tau, \tag{35}$$

and from the Wagner condition (21) we then have

$$\frac{d_I(t)^2}{2} = \int_0^t \frac{d_I(t)}{\sqrt{d_I(t)^2 - d_I(\tau)^2}} \mathrm{d}\tau. \tag{36}$$

This is an integral equation for $d_I(t)$ and has unique positive solution $d_I(t) = 2t^{\frac{1}{2}}$ (again in line with [24]). Hence from (35) we now know

$$h_I(x,t) = -t + \frac{x^2}{2} - \frac{|x|}{2}\left(x^2 - 4t\right)^{\frac{1}{2}}. \tag{37}$$

Consequently from (13) the unknown free-surface shape is now found to be

$$\eta_I(x,t) = \frac{x^2}{2} - h_I(x,t) = t + \frac{|x|}{2}\sqrt{x^2 - 4t}, \qquad |x| \geq d_I(t). \tag{38}$$

As $|x| \to \infty$, $\eta_I \sim \frac{x^2}{2} - \frac{t^2}{x^2}$, and the velocity potential follows from (32)

$$\phi_{I,x}(x,0,t) = \frac{x}{\sqrt{d_I(t)^2 - x^2}}. \tag{39}$$

Integrating from $x = d_I$ to x (where $|x| < d_I$), we have

$$\phi_I(x, 0, t) = -\sqrt{d_I(t)^2 - x^2}. \tag{40}$$

From (37), $h_I \sim \frac{t^2}{x^2}$ as $|x| \to \infty$. From (38), we conclude that the liquid surface bulges out owing to the substrate striking it upwards from below. The partial t-derivative of (40) gives an expression for $p_{lI} = -\phi_{I,t}$, the pressure on the substrate surface. The pressure

$$p_{lI}(x, 0, t) = \frac{d_I \dot{d}_I}{\left(d_I^2 - x^2\right)^{\frac{1}{2}}} \qquad |x| < d_I, \tag{41}$$

which is singular at $x = \pm d_I$, and where $\dot{d}_I$ denotes the time derivative. Note that $d_I \dot{d}_I = 2$ is independent of t so that p_{lI} is singular at $x = 0$, at $t = 0$, but that the product of d_I and p_{lI} is non-singular in boundary condition (23) used in the next section.

3.3 Porous contribution

We now look for the first order ($O(k)$) correction to the leading order Wagner solution ($k = 0$) for the model described in Sect. 3.1. We now allow the liquid in the droplet to penetrate into the substrate such that the velocity on the wetted boundary of the substrate is subject to condition (23) as discussed in §3.1. Under the assumption that $k \ll 1$, we introduce the asymptotic expansions (24)–(26). The expansion for $d(t)$ is not trivial. If we keep a general expansion of the form $d(t) = 2t^{\frac{1}{2}} + kd_p(t) + O(k^2)$, in keeping with the other unknowns, then the proposed balance is found to be mathematically consistent only when the power is one-half in $d_p(t) = at^{\frac{1}{2}}$ for some constant a. Finding the value of a and the functions h_p and ϕ_p remains our challenge.

Following the same complex analysis approach from above, governing equation (33) becomes

$$\left(h_I + kh_p\right)_t = \frac{1}{\pi\sqrt{x^2 - d^2}} \int_{-d}^{d} \frac{\sqrt{d^2 - \alpha^2}(1 + k\mathrm{d}\phi(\alpha, t)_t)}{\alpha - x} \mathrm{d}\alpha \tag{42}$$

$$= \frac{1}{\pi\sqrt{x^2 - d^2}} \int_{-d}^{d} \frac{\sqrt{d^2 - \alpha^2}(1 + k\mathrm{d}\phi_I(\alpha, t)_t)}{\alpha - x} \mathrm{d}\alpha \tag{43}$$

$$= \frac{1}{\pi\sqrt{x^2 - d^2}} \left(\int_{-d}^{d} \frac{\sqrt{d^2 - \alpha^2}}{\alpha - x} \mathrm{d}\alpha + k \int_{-d}^{d} \frac{d\sqrt{d^2 - \alpha^2}\phi_I(\alpha, t)_t}{\alpha - x} \mathrm{d}\alpha \right), \tag{44}$$

where $d = d(t)$ and we neglect higher order terms in k.

The first integral is similar to the impermeable case, except that d is no longer d_I. Using the t-derivative of the known ϕ_I from (40) the second integral becomes

$$\frac{kd^2\dot{d}}{\pi\sqrt{x^2-d^2}}\int_{-d}^{d}\frac{\sqrt{d^2-\alpha^2}}{\sqrt{d^2-\alpha^2}(\alpha-x)}\mathrm{d}\alpha = \frac{kd^2\dot{d}}{\pi\sqrt{x^2-d^2}}\int_{-d}^{d}\frac{1}{\alpha-x}\mathrm{d}\alpha, \tag{45}$$

$$= \frac{kd^2\dot{d}}{\pi\sqrt{x^2-d^2}}\log\left|\frac{d-x}{d+x}\right|, \tag{46}$$

which is valid for $|x| > d$. Thus (44) can be written as an expression for the free-surface displacement, as

$$h_{I,t} + kh_{p,t} = -1 + \frac{x}{\sqrt{x^2-d^2}} + \frac{kd^2\dot{d}}{\pi\sqrt{x^2-d^2}}\log\left|\frac{d-x}{d+x}\right|, \tag{47}$$

for $x > d$ and neglecting higher order terms.

Thus far we have kept the form of the asymptotic expansion of d as general as possible. It is possible to continue the analysis further with arbitrary d, however the required application of the Wagner condition (21) at some stage then enforces $d_I(t) \sim t^{\frac{1}{2}}$ and thus $d(t) = (2+ka)t^{\frac{1}{2}}$ for mathematical consistency. We adopt this requirement from this point onwards to simplify the workings below.

To obtain $h(x,t)$ we integrate (47) with respect to t' from 0 to t. For convenience, we use a change of integration variable on the log term by writing

$$t' = \frac{d'^2}{(2+ka)^2}, \tag{48}$$

obtaining

$$h(x,t) = h(x,0) - t + \frac{2x^2}{(2+ka)^2} - \frac{2|x|\sqrt{x^2-d^2}}{(2+ka)^2} + \frac{k}{\pi}\int_0^d \frac{d'^2}{\sqrt{x^2-d'^2}}\log\left|\frac{d'-x}{d'+x}\right|\mathrm{d}d', \tag{49}$$

where $h(x,0) = 0$. We rewrite the final term in the integral in a compact form:

$$h_I + kh_p = -t + \frac{2x^2}{(2+ka)^2} - \frac{2|x|\sqrt{x^2-d^2}}{(2+ka)^2} + \frac{k}{\pi}x^2F\left(\frac{d}{x}\right), \tag{50}$$

where the final term is a function of d/x only.

By making the substitution $d = Sx$, and defining $f(S) = (1-S^2)^{\frac{1}{2}}\log\left(\frac{1-S}{1+S}\right)$ and integrating by parts, some algebra (see Appendix A for the details) leads to

$$F\left(\frac{d}{x}\right) = -\frac{d}{|x|}\left(1-\frac{d^2}{x^2}\right)^{\frac{1}{2}}\log\left(\frac{x-d}{x+d}\right) + \left(1-\frac{d^2}{x^2}\right)^{\frac{1}{2}} - 2 + \int_0^{\frac{d}{x}} f(S)\mathrm{d}S. \tag{51}$$

We can now apply the Wagner condition (21), namely

$$\frac{d^2}{2} - t = h(d, t). \tag{52}$$

Evaluating (51) and (49) at $x = d$, condition (52) becomes

$$\frac{d^2}{2} - t = -t + \frac{2d^2}{(2+ka)^2} - \frac{d^2 k}{\pi}\left(2 - \int_0^1 f(S)\mathrm{d}s\right). \tag{53}$$

Evaluation of the integral is a numerical task, and we find that $c = \int_0^1 f(S)\mathrm{d}s = -0.832$ to three significant digits using the trapezium rule. The expressions give us

$$\frac{d^2}{2} = \frac{2d^2}{(2+ka)^2} - \frac{d^2 k}{\pi}(2-c) + O(k^2) \tag{54}$$

in which by design of d, every term is directly proportional to t. After cancelling factor d^2, we have

$$\frac{(2+ka)^2}{2} = 2 - \frac{k}{\pi}(2-c)(2+ka)^2 + O(k^2). \tag{55}$$

Hence

$$a = -\frac{2}{\pi}(2-c) + O(k). \tag{56}$$

Neglecting the $O(k)$ contribution leaves $a = -1.803$, an $O(1)$ coefficient. In summary, we have shown that

$$d(t) = (2 - 1.803\,k)\,t^{\frac{1}{2}}. \tag{57}$$

Since a is negative, the porous contact region is smaller and spreads more slowly than for the impermeable substrate. This is intuitive since the incompressible fluid can enter the substrate leaving less liquid to spread across the surface.

Returning to (13), the free-surface position is

$$\eta(x,t) = \frac{x^2}{2} + t - \frac{2x^2}{(2+ka)^2} + \frac{2|x|\sqrt{x^2-d^2}}{(2+ka)^2} - \frac{k}{\pi}x^2 F\left(\frac{d}{x}\right), \tag{58}$$

valid at first order in k, for $|x| \geq d$. Setting $k = 0$ returns this to the impermeable result (38) with $d = 2t^{\frac{1}{2}}$. Here $F(d/x)$ is defined by (51) The velocity potential in the wetted region $|x| \leq d$ follows in a similar manner yielding

$$-\phi_I(x,0,t) - k\phi_p = \sqrt{d^2-x^2} - \frac{kd(2+ka)^2}{2\pi}\int_x^d (d^2 - x'^2)^{-\frac{1}{2}} \log\left|\frac{d-x'}{d+x'}\right| \mathrm{d}x', \tag{59}$$

where $\phi_I(x, 0, t)$ is given by (40), and $d(t)$ is given by (57). The integral can be simplified and approximated numerically (see Appendix B for details). In appendices A and B the integral is re-expressed with an approximation which can be diffentiated with respect to x or t. The t derivative of (59) gives us the liquid pressure present in the boundary condition (23) from which we determine the fluid velocity into the substrate-again see Appendix B for the complete expression (B8).

4 Results

We present and discuss our results for the free surface and the turnover position, the velocity potential, pressure distribution and liquid injection into the porous substrate. In each case we show the quantity as a function of position, $x \in [0, d]$, and selected times $t > 0$. The results are symmetric in x so we only report the right half of the domain. Our aim is to compare and contrast the results for a porous substrate with those for an impermeable surface. In each case we highlight the influences of porosity on the flow, compared with the impermeable case. Throughout, every porous-substrate calculation is done with the same value for the porosity parameter, $k = 0.1$, and impermeable results correspond to $k = 0$.

4.1 Free surface motion, turnover position and pressure

Figure 3 shows the free-surface shape and pressure distribution for $x \in [0, d)$ at selected times for $k = 0.1$. The model is symmetric in x, so we show the right-half alone. In Fig. 3a, as $y \to \infty$ the surface is at rest. As t increases the surface moves towards the right. The droplet bulges out. On the horizontal substrate, the turnover point accelerates to the right along the boundary, with position $x = d(t)$, $y = 0$, on the substrate.

In Fig. 3b, there is a mild square-root singularity at $x = d_I$ in the pressure (along with an even milder, logarithmic singularity at $x = d$ for the porous-substrate results, not shown). At $x = 0$ the pressure, $p(0, 0, t)$ is singular at the instant of first contact, $t = 0$. Thereafter the pressure at $x = 0$, $p(0, 0, t)$, decreases monotonically in time towards zero. Elsewhere, at any fixed station x, there is a time-delay before the fluid arrives, at time t_*, where $d(t_*) = x$. At any fixed time, the spatial distribution of impermeable-substrate pressure, $p_I(x, 0, t)$, has a *global minimum at the origin*, and p_I increases monotonically towards a positive singularity at $x = d$. Nearer the turnover point, for the region $x \in (0.7d, d)$, the pressure tends to plus infinity, due to the square-root factor in the leading order term for pressure, $d\dot{d}/\sqrt{d^2 - x^2}$, as x increases to d. See Appendix B. What we do not see in Fig. 3 is the milder logarithmic singularity at $x = d$, present in the $O(k)$ porous-contribution term. This term describes a marked lowering in pressure near the edge of the domain.

Figure 4 compares the standard impermeable Wagner solution, with the porous model developed here. For the times shown, the porous-case free surface moves more slowly than the impermeable case. Note that at any instant, $0 < d < d_I$ and $0 < \dot{d} < \dot{d}_I$, where subscript I denotes the impermeable case. Comparing results

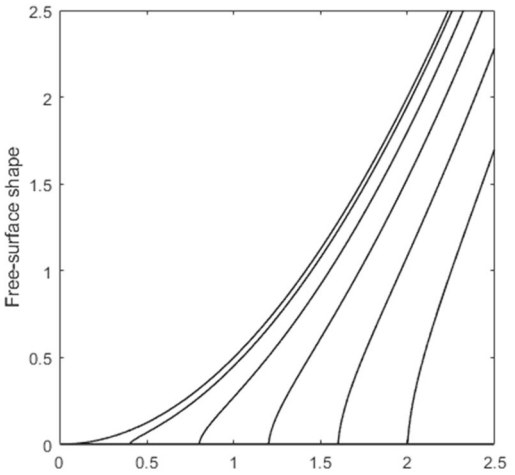

(a) Free-surface shapes $\eta(x,t)$ as a function of x, at selected increasing times $t = 0, 0.2, 0.4.0.6, 0.8, 1$.

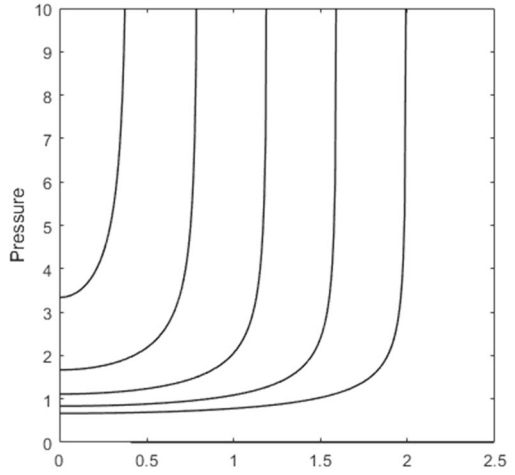

(b) Pressure profiles in x, at selected times $t = 0, 0.2, 0.4.0.6, 0.8, 1$

Fig. 3 Figures showing the solution to the Wagner problem with the porous boundary conditions with $k = 0.1$ with **a** the free-surface η and **b** the pressure p for $0 \leq x \leq d_I(t)$

for impermeable and porous cases is awkward owing to the difference between the turnover positions $x = d_I(t)$ and $x = d(t)$. For $k = 0.1$, we find d_I exceeds d by about 9%, at all times plotted in Fig. 4.

There are visible differences in the shape of the free surface too, especially near the turnover point. For impermeable substrate the droplet's surface meets the solid orthogonally—the contact angle, evaluated inside the fluid, is exactly 90^0. For the porous-substrate, the droplet's surface meets the plate with an obtuse contact angle, more than 90^o. By the last time plotted, the angle has increased to about 96 ± 2^0. This increase in angle is related to a loss of fluid from the drop into the substrate.

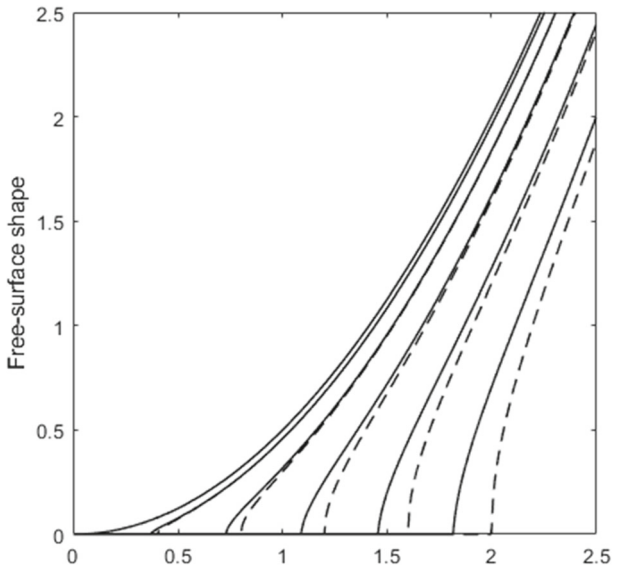

Fig. 4 A free-surface comparison of η between the impermeable solution (dashed) and the porous solution (solid) for $k = 0.1$. Selected times are $t = 0, 0.2, 0.4.0.6, 0.8, 1$

4.2 Velocity potential

Focussing on the substrate surface $y = 0$, Fig. 5 shows minus velocity potential, $-\phi(x, 0, t)$, as a distribution in space at selected times, and for shared values of $d = 0.4, 1.2, 2$ (corresponding to differing times). Every curve has one global maximum, at $x = 0$. Also, in keeping with a boundary condition, $-\phi$ is zero at $x = d$. At the edge of the impact region, $x = d$, the curve always has a vertical tangent, indicating the high velocity associated with the outer region matched to the inner jet-root region in Wagner theory.

The dashed curves in Fig. 5 are the impermeable results, and the solid curves mark the corresponding porous results. The figure shows that porosity acts to reduce the value of $-\phi$; the liquid impact is less violent. This is to be expected on physical grounds, because the liquid pressure is relieved by its work of injecting fluid into the substrate. For $k = 0.1$, the reduction in $-\phi$ is about 27%. The reduction in $-\phi$ is proportional to k, but in a complicated way, as shown in equation (B5).

The velocity potential is central to any discussion of the fluid mechanics of our results because its partial $x-$ and $t-$ derivatives give the horizontal velocity component and the pressure at the substrate's surface, respectively. Incidentally, $-\phi(x, 0, t)$ is directly proportional to the pressure-impulse for the droplet impact over the time interval $[0, t]$, and can be read as a local measure of impulsive force per unit length of substrate (see Sect. II of [37]).

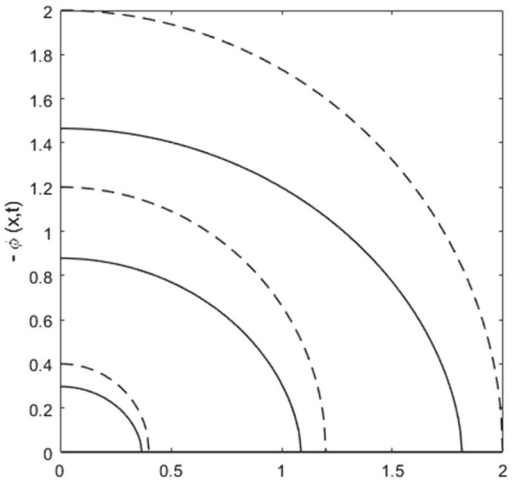

(a) $-\phi$ compared at equal times $t = 0.2, 0.6, 1.0$.

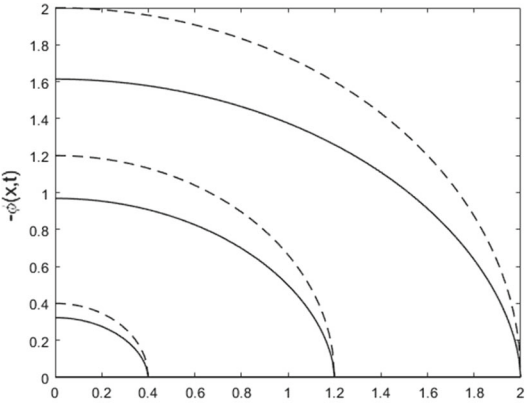

(b) $-\phi$ compared at three equal contact line positions $d(t)$.

Fig. 5 Comparisson of the velocity potential ϕ between porous (solid) and impermeable (dashed). For each curve, $\phi = 0$ coincides with the turnover point $x = d(t)$

4.3 Liquid penetration of the substrate

At $y = 0$ the porous boundary condition (23) models the upward vertical velocity component, relative to the substrate. So the downward velocity is $v(x, 0, t) = k\, d(t)\phi_t(x, 0, t)$. This positive quantity is shown in Fig. 6. Panel (a) shows the distribution of v in space, at five instants in time. A singularity at $x = d$ highlights the transient influence of high-pressure liquid being injected into the substrate during impact. Figure 6(b) shows v as a function of time at two fixed stations x. Each plotted curve includes a waiting-time interval, $[0, t_w]$, until the fluid arrives, where t_w is defined by $d(t_w) = x$. First, the singularity (in pressure and hence v) arrives and quickly sweeps past the x-station. Afterwards the penetration velocity decreases rapidly towards zero, but over the theory's limited $O(1)$ time, the plot shows only a modest decline.

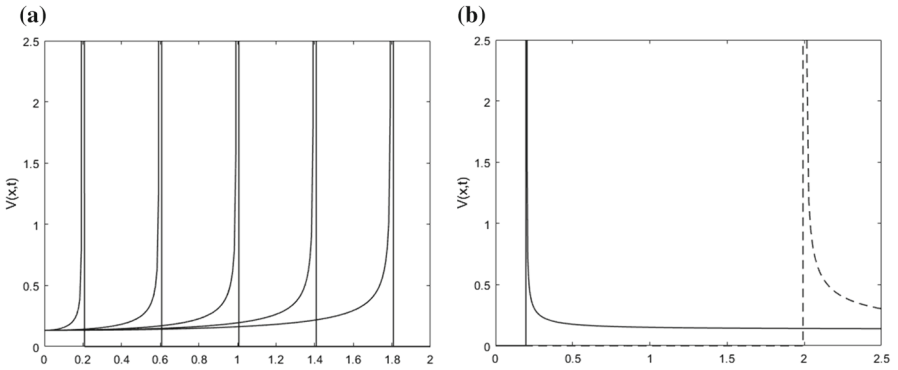

Fig. 6 Plot showing the fluid velocity into the substrate at **a** as a function of x at 5 fixed times (left) and **b** as a function of time at 2 fixed x locations (right)

We are interested in the accumulated effect of the highly transient behaviour of v. We represent this by a flux $q(x,t)$ of fluid that passes through the boundary up to current time t. Here we define q as

$$q(x,t) = \int_{t_w}^{t} -v(x,0,t')\,\mathrm{d}t' = -k\int_{x}^{d} d'\,p\,\frac{1}{\dot{d}'}\,\mathrm{d}d'. \tag{60}$$

The integral's lower limit in (60) marks the end of the waiting-time t_w before the arrival of fluid. To $O(k)$, the pressure has only one term and the factor $\dot{d}$ in the integral cancels with the same factor in p—see Appendix B expression (B8). So this leaves us with

$$q(x,t) = k\int_{x}^{d} \frac{d'^2}{(d'^2 - x^2)^{1/2}}\,\mathrm{d}d' + O(k^2). \tag{61}$$

A substitution $d' = x\cosh(s)$ enables conversion to a straightforward s-integral, which we evaluate in terms of variable $\xi = x/d$. Hence

$$q(x,t) = \frac{1}{2}k\,d^2\left(\xi^2\mathrm{arccosh}(|\xi|^{-1}) + [1-\xi^2]^{1/2}\right) \qquad -1 \le \xi \le 1, \tag{62}$$

where $\xi = x/d$. The time dependence comprises a compound of two increasing parts in (62). First, the factor $d^2 = (2+ka)^2 t$ increases linearly. Secondly, for each fixed x, the value of $\xi = x/d$ decreases in time, and we find the factor in round brackets in (62) increases monotonically towards one. The net effect is a monotonic increase in q with time.

In terms of spatial distribution of $q(x,t)$ in (62), the term in large round brackets defines the following function

$$E(\xi) = \xi^2\mathrm{arccosh}(|\xi|^{-1}) + (1-\xi^2)^{1/2} \qquad -1 \le \xi \le 1. \tag{63}$$

Note that $E \to 1$ as $\xi \to 0$. Also $E(\xi)$ is universal and independent of k.

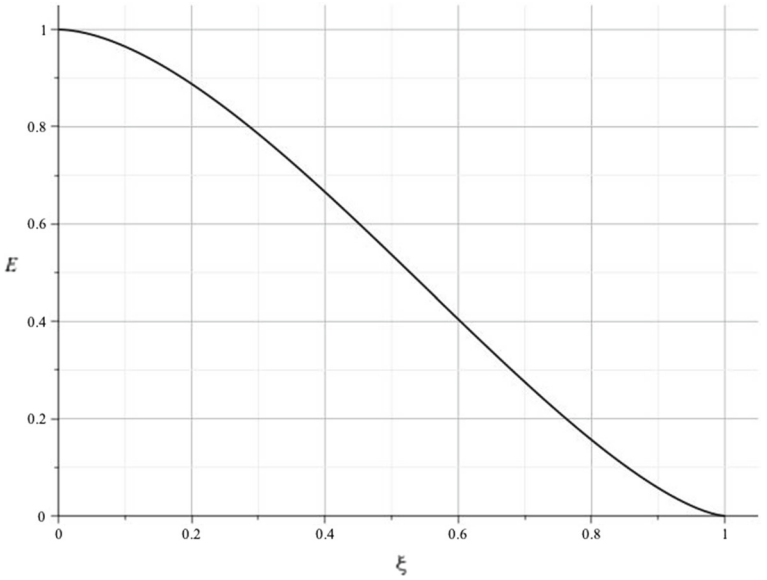

Fig. 7 Spatial distribution of liquid injected into the substrate up to current time t. Plotted is $E(\xi) = q(x,t)/(\frac{1}{2}\,k\,d^2)$ from (63), where $\xi = x/d(t)$

A plot of $E(\xi) = q/(\frac{1}{2}\,k\,d^2)$ is shown in Fig. 7. The net flux q has a single maximum at $x = 0$, and declines in space towards the edge of the domain. This kind of behaviour accords with our expectations on physical grounds: the penetration of fluid is most intense, and endures longest, at the centre of the impact zone. An important observation is an absence of singularities in the plot or expression (62). The time-integration carried out above, annuls the singularity in pressure at $x = d$.

Indeed q *is zero* at $x = d$. The flux tails off towards the edge of the impact zone in Fig. 7. The physical consequence of our theory, on what might be measured, is significant. Near the edge of the impact zone, and despite a passing singular pressure, there has been too little time yet to force into the substrate a significant amount of liquid. We have shown that, at all times, $q = 0$ at $x = d$.

We take this analysis one stage further and (numerically) integrate $q(x,t)$ with respect to x from $-d$ to d, to obtain the total area $Q(t)$ of fluid injected into the whole substrate, by the impact up to time t. This is

$$Q(t) = \int_{-d}^{d} q(x,t)\,\mathrm{d}x = 2\frac{1}{2}\,k\,d^3 \int_0^1 E(\xi)\,\mathrm{d}\xi = 0.5236\,k\,d^3, \tag{64}$$

where the dimensionless coefficient is evaluated to high precision, and quoted to 4 significant digits.

The area (volume per unit width in third dimension) of fluid, Q, increases directly proportional to $k\,t^{3/2}$. If we set an $O(1)$ upper limit on time, then (64) supplies an expected total area of fluid, that can end up inside the substrate after the impact has finished. From our expression $d(t) = (2 + ka)t^{1/2}$, and for a range of small values of

$k \in [0, 0.1]$, we expect $Q(t)$ to lie in the interval $[0, 0.3155\, t^{3/2}]$. Consistent with our asymptotic analysis, the coefficient is $O(1)$; it is evaluated to 4 significant digits.

Having presented our main results, the next section models a consequence of our solution in the main outer region, for the flow in the inner region at the edge of the impact zone, consisting of the splash jet and its root.

5 Jet-root and jet regions

The solution for the porous model exhibits the same singular behaviour in the pressure at the turnover points as the impermeable case. This singularity is resolved by rescaling, considering an $O(\epsilon^2)$ region in the neighbourhood of the turnover point, usually referred to as the jet-root region. In Wagner theory this reveals a fast-moving thin jet that flows horizontally across the surface of the substrate far quicker than the spreading turnover point. The neighbourhood of $x = d$ is examined using variables with subscript j (for "jet"). The rescaling is as follows:

$$x = d(t) + \epsilon^2 x_j, \tag{65}$$

$$y = \epsilon^2 y_j, \tag{66}$$

$$t = t_j, \tag{67}$$

$$\phi = \epsilon \left(\phi_j + \dot{d} x_j\right), \tag{68}$$

where the subscript j refers to jet variables, and $\dot{d}$ denotes the time derivative. The free surface position $y_j = \eta_j$ is $O(1)$ in this rescaled region and so our boundary conditions are no longer linearised onto $y = 0$. We consider the solution for the velocity potential (59) and we substitute our new scaled variables into this equation to obtain a far-field matching condition for the local jet solution. With some effort, it can be demonstrated that the contributions of the integral in the expression for ϕ in (59) will never appear at leading order even without our additional restriction of k being small. In fact, we require

$$\phi_j(x_j, 0, t) \to \sqrt{-2d x_j} - \dot{d} x_j, \tag{69}$$

in the far-field to match with ϕ. See Appendix C for details.

We also have our substrate boundary condition (23) which, after substituting in our new scaled variables, leaves simply

$$\phi_{j\, y_j} = 0 + O(\epsilon), \tag{70}$$

meaning the substrate condition has zero direct influence on the problem on this smaller length scale, and it collapses back to being unchanged from impact onto an impermeable substrate.

The influence of porosity is still felt through the far-field matching condition on the velocity potential ϕ_j to ensure it matches with the outer solution, where the global influence of porosity is recovered via changes in d. A similar effect is seen in this jet

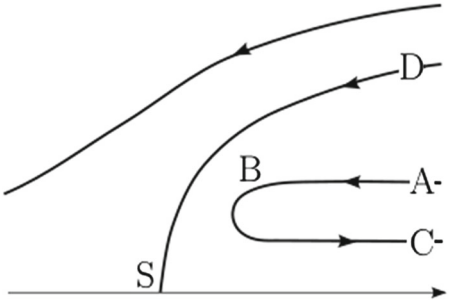

(a) Geometry of the local jet-root region, with streamlines viewed in a frame moving horizontally with the turnover point B. A stagnation point is marked as S. The free-surface streamline is AC.

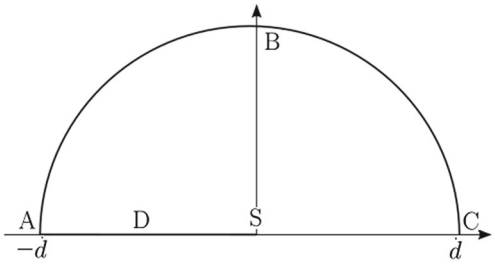

(b) Hodograph plane of velocity components within a semicircular region.

Fig. 8 **a** Local jet root region, and **b** mapped domain in the hodograph plane. Upper case letters mark corresponding points

root region during impact onto elastic substrates, where the influence of the flexible substrate behaviour is again only passively felt via the far-field matching (see [28]).

On the free surface the boundary condition becomes

$$\phi_{j_n} = \epsilon \eta_{j_t} = 0 + O(\epsilon), \tag{71}$$

where n is the coordinate normal to the free-surface.

The jet model governing equations in x_j, y_j coordinates are

$$\nabla^2 \phi_j = 0 \qquad \text{in the droplet,} \tag{72}$$

$$\phi_{j,y_j} = 0 \qquad \text{on flow boundaries,} \tag{73}$$

$$\left|\nabla \phi_j\right| = \dot{d} \qquad \text{on the free surface.} \tag{74}$$

See also Fig. 8a. To solve this system we use a hodograph plane method in which the coordinates are the velocity components, and the fluid domain is the semicircular region shown in Fig. 8b. We define a complex potential $W = \phi_j + i\psi_j$ and the complex velocity $U = \frac{\mathrm{d}W}{\mathrm{d}\zeta} = \phi_{j,x_j} - i\phi_{j,y_j}$ with $\zeta = x_j + iy_j$. The complex velocity plane corresponds to the semi-circle ${\phi_{j,x_j}}^2 + {\phi_{j,y_j}}^2 = \dot{d}^2$ with $-\phi_{j,y_j} > 0$. In the far field as $x_j^2 + y_j^2 \to \infty$, we require $U = -\dot{d}$ as, since we are in a frame of reference moving with the turnover point, the far-field is steady. We assume the jet approaches a

uniform thickness in space, H_j as $x_j \to \infty$, which grows in time. From the dynamic boundary condition (74) we have $\phi_{j,y_j} \to 0$ and $\phi_{j,x_j} \to \dot{d}$ as $x_j \to \infty$. The kinematic condition (73) requires that the stream function is independent of x_j and y_j on the fluid interface. We take $\psi_j(x_j, y_j, t) = 0$ on the substrate-liquid interface and $\psi_j(x_j, y_j, t) = f_l(t)$ on the free surface, where $f_l(t)$ is unknown.

In this quasi-steady flow, velocity is tangent to the jet free-surface and of magnitude $\dot{d}$. Since the jet free surface is horizontal in the far field, this requires,

$$\phi_{j,x} = \psi_{j,y} = \dot{d}, \tag{75}$$

valid in the far-field. Integrating with respect to y yields the value of ψ_j on the free surface:

$$f_l(t) = \dot{d} H_j, \tag{76}$$

where $H_j = H_j(t)$ only.

From the matching condition (69), and replacing x_j by the complex variable ζ we have as $x_j \to -\infty$:

$$W(\zeta) \sim \sqrt{-2d\zeta} - \dot{d}\zeta, \tag{77}$$

and, the complex velocity is therefore

$$U(\zeta) = \frac{\mathrm{d}W}{\mathrm{d}\zeta} \sim -\dot{d} - d(-2d\zeta)^{-\frac{1}{2}}. \tag{78}$$

Rearranging, we have

$$\zeta \sim \frac{-1}{2d}\left(\frac{\dot{d}+U}{d}\right)^{-2}. \tag{79}$$

Substituting this into (77) to eliminate ζ we have

$$W = \frac{\dot{d}d}{2}\left(\dot{d}+U\right)^{-2} + \frac{d}{\dot{d}+U} \sim \frac{\dot{d}d}{2}\left(\dot{d}+U\right)^{-2}, \tag{80}$$

as $U \to -\dot{d}$. This is a condition on $W = W(U)$, still to be found.

Next we construct W. Consider

$$U = \frac{dW}{d\zeta} = \frac{dW}{dU}\frac{dU}{d\zeta}. \tag{81}$$

At the stagnation point $U = 0$, (81) tells us that dW/DU is zero there, because $dU/d\zeta$ cannot vanish for a conformal mapping from the physical ζ plane to the hodograph U

plane. We split W into a sum of two parts, let $W(U) = W_1(U) + W_2(U)$, with

$$W_1 = -\frac{dU(U+\dot{d})^{-2}}{2}, \tag{82}$$

$$W_2 = -\frac{2f_l(t)}{\pi}\log\left(\frac{\dot{d}-U}{\dot{d}+U}\right), \tag{83}$$

with W_1 having a strong singularity in order to match with the correct behaviour in (80) as $U \to -\dot{d}$ on the in-flowing part of the domain, and W_2 describes a sink as $U \to \dot{d}$ and a source as $U \to -\dot{d}$. We have the condition at the stagnation point $\frac{dW}{dU} = 0$, so we have

$$\frac{dW_1}{dU} + \frac{dW_2}{dU} = 0. \tag{84}$$

From (82) and (83), at $U = 0$, we find exactly that

$$f_l(t) = \frac{\pi d}{8\dot{d}}. \tag{85}$$

From (76) we deduce that the jet thickness depends on $d(t)$ as follows:

$$H_j(t) = \frac{\pi d(t)}{8\dot{d}(t)^2}. \tag{86}$$

With (57),we expand $H_j(t)$ in powers of k:

$$H_j(t) = \frac{\pi t^{\frac{3}{2}}}{2}\frac{1}{2-1.803k}, \tag{87}$$

$$H_j = \frac{\pi}{4}t^{\frac{3}{2}}\left(1 + \frac{1.803}{2}k + O(k^2)\right). \tag{88}$$

Note that in terms of the outer variables the top of the jet lies at $y = \epsilon^2 H_j(t)$. We have shown that the effect of the porous substrate is to thicken the splash jet, and slow it down.

Since the jet is thicker and slower, the question remains as to whether the porosity changes the volume flux of fluid entering the jet? The volume flux of the jet can be calculated by integrating the velocity of the jet over its thickness giving the value of the stream function on the upper surface of the jet:

$$\psi_j = \int_0^{H_j} \dot{d}(t)\mathrm{d}y = \dot{d}H_j = \frac{\pi t}{4}. \tag{89}$$

Also $\psi = 0$ on $y = 0$. So the flux into the jet is independent of k, equal to the flux of the jet on a impermeable substrate, and hence unchanged by the porosity.

For completeness, we also mention that there is a further asymptotic jet region. As the flow leaves the jet-root region described above, it enters a long thin jet with thickness remaining $O(\epsilon^2)$, but with a longer horizontal scale. A suitable scaling of the coordinates leads to governing shallow water equations, with boundary conditions given by

$$\hat{u}(d,t) = 2\dot{d}(t) \qquad \text{and} \qquad \hat{h}(d,t) = H_j(t) \tag{90}$$

for the horizontal jet velocity $\hat{u}(x,t)$, and thickness $\hat{h}(x,t)$. Full details can be found in [23]. It is found that this jet region is entirely passive, and is of infinite horizontal extent for the impact of liquid and solid bodies bounded by a smooth surface before impact where $\dot{d} \to \infty$ as $t \to 0$. Complications can occur for impact of non-smooth bodies (for example a cone where the jet is found to be of finite extent, see [24]), and also for impact onto flexible elastic substrates (where large oscillations in $d(t)$ can lead to unbounded growth in the thickness $h(x,t)$ in the jet region and hence the subsequent breakdown of the shallow water model, see [28]). Details for the current porous model are omitted as the solution in this region remains largely unchanged from the impermeable case, except for the correction to the thickness and speed at the turnover point.

6 Conclusions

In this paper, we have introduced porosity to the standard Wagner model of droplet impact onto an impermeable substrate, via a boundary condition designed to closely mimic a full Darcy theory model of a porous substrate. An analytical solution to the problem in the limit of small porosity has been derived and results have been presented for the outer problem showing how the inclusion of porosity slows the spreading of the droplet, changes the evolution of the free-surface shape, reduces the maximum pressure, and drives fluid into the substrate. A local analysis of the jet-root region reveals that, compared to impermeable impact, the fast moving jet travelling along the substrate is thicker and slower while keeping the flux unchanged. This last result is perhaps the most surprising finding from the study; to us there is no obvious physical reason for this. While results have been presented for just one k value, and the asymptotic approach in Sect. 3.3 restricts the solution to small k, the boundary condition is applicable for arbitrary k. Solving for arbitrary k is likely a numerical task, but it would be interesting to see how the small k features identified here persist for larger k.

The current model has been restricted to two-dimensions for this initial study. It is expected that extending our model into the more realistic scenario of axisymmetry flow should be achievable with a generalised version of our boundary condition (23), a similar small porosity expansion, and the axisymmetric Wagner analysis originally presented by [24].

Experimental validation of our results is hard to find. Many published studies into impact onto porous beds focus on erosion or powders [7, 10, 18–20]. Could our prediction of a slower and thicker jet be tested by comparision with future experiments?

Likewise, can the volume-flux distribution in Fig. 7 be investigated experimentally? Numerical validation would also be of great use. Numerical solutions have validated Wagner models in various configurations, including impact onto moving substrates [38], and detailed numerical solutions for comparison with our results would be welcomed.

One main purpose of this study was a first step towards a fully coupled Wagner-Darcy model for droplet impact onto a porous substrate. Looking ahead, such a model is relatively easy to formulate within the flow structure described here. The porous boundary condition (23) is replaced by a coupling condition for the fluid pressure with a suitable porous flow model in the substrate. Various limiting cases exist for the Darcy flow depending on whether or not the depth of the substrate is similar to the outer or local length scales in the Wagner region. Solutions for saturated, unsaturated and partially saturated substrates are all of interest with differing challenges and applications. A more detailed discussion of the formulation, including these differing regimes, can be found in the further work discussion of [34]. It is reassuring for potential progress towards a solution in this more complicated actively coupled case that the standard Wagner structure in two-dimensional and axisymmetric geometries appears to still hold, in particular in the local jet root region.

Author contributions The authors jointly worked on the analysis and calculations, discussed the results, and wrote and reviewed the manuscript.

Declarations

Conflict of interest The authors declare no conflict of interest.

Appendix A: Re-expression of $F(d/x)$

Here we focus on the integral in (49). To transform this integral into something more tractable, we let $d = Sx$, $f(S) = (1-S^2)^{\frac{1}{2}} \log\left(\frac{1-S}{1+S}\right)$ and $G(S) = \log\left(\frac{1-S}{1+S}\right)$ so we have

$$x^2 F\left(\frac{d}{x}\right) = \int_0^d \frac{d'^2}{\sqrt{x^2-d'^2}} \log\left(\frac{x-d'}{x+d'}\right) \mathrm{d}d' \qquad \text{for} \quad |x| > d$$
$$= \int_0^{\frac{d}{x}} \frac{x^2 S^2}{\sqrt{1-S^2}} G(S) \mathrm{d}S \tag{A1}$$

Dividing both sides by x^2 and integrating by parts gives

$$F\left(\frac{d}{x}\right) = x^2\left([-Sf(S)]_0^{\frac{d}{x}} - \int_0^{\frac{d}{x}} -(1-S^2)^{\frac{1}{2}}\left(G(S) - \frac{S}{1-S} - \frac{S}{1+S}\right)\mathrm{d}S\right)$$

$$= -\left(1-\frac{d^2}{x^2}\right)^{\frac{1}{2}}\frac{d}{x}\log\left(\frac{x-d}{x+d}\right) + \int_0^{\frac{d}{x}} f(S) - (1-S^2)^{\frac{1}{2}}\frac{2S}{1-S^2}\mathrm{d}S \tag{A2}$$

$$= -\frac{d}{x}\left(1-\frac{d^2}{x^2}\right)^{\frac{1}{2}}\log\left(\frac{x-d}{x+d}\right) + \left[2(1-S^2)^{\frac{1}{2}}\right]_0^{\frac{d}{x}} + \int_0^{\frac{d}{x}} f(S)\mathrm{d}S$$

$$F = -\frac{d}{x}\left(1-\frac{d^2}{x^2}\right)^{\frac{1}{2}}\log\left(\frac{x-d}{x+d}\right) + 2\left(1-\frac{d^2}{x^2}\right)^{\frac{1}{2}} - 2 + \int_0^{\frac{d}{x}} f(S)\mathrm{d}S. \tag{A3}$$

For all t, as $x \to \infty$, it can be shown with care that $F \to 0$ as expected, as x increases the log term vanishes and the limits of the integration tend to zero.

Appendix B: Evaluation of the velocity potential and pressure

To approximate (59) we write

$$-\phi(x,0,t) = \sqrt{d^2-x^2} + \frac{kd(2+ka)^2}{2\pi}\int_x^d (d^2-x'^2)^{-\frac{1}{2}}\log\left(\frac{d-x'}{d+x'}\right)\mathrm{d}x'. \tag{B4}$$

Substitution of $x' = d\cos(\theta)$ simplifies the integrand, and leaves:

$$-\phi(x,t) = \sqrt{d^2-x^2} - \frac{kd(2+ka)^2}{2\pi}\int_{\arccos(\frac{x}{d})}^0 2\log\left(\tan\left(\frac{\theta}{2}\right)\right)\mathrm{d}\theta. \tag{B5}$$

The form of (B5) allows us to differentiate it with respect to x or t. We find an approximation of the integral

$$I = 2\int_{\arccos(\frac{x}{d})}^0 \log\left(\tan\left(\frac{\theta}{2}\right)\right)\mathrm{d}\theta, \tag{B6}$$

Writing $\tan(\theta/2)$ as a rational approximation from Weierstrass's infinite products for $\sin(\theta/2)$ and $\cos(\theta/2)$ we have

$$\log\left(\left|\tan\left(\frac{\theta}{2}\right)\right|\right) \approx \log\left(\pi^2\left(1-C^2\theta^2\right)\right) + \log\left(\frac{\theta}{2}\right) - \log(\pi-\theta) - \log(\pi+\theta), \tag{B7}$$

with $C = 0.1341187916$ and the coefficient of the $O(\theta^4)$ term being negligible. The integral is best approximated near $\theta = 0$, and near the closest singularities at $\theta = \pm\pi$.

We can now integrate (B6) by using standard methods. Comparison between the approximation of the integral (B6) using the expansion (B7), and a direct numerical integration method shows the difference is very small (less than 1%). Hence, (B7) is used throughout the calculations presented in this paper.

The fluid pressure on the substrate, given by the time derivative of the velocity potential, can be similarly expressed in the form

$$p = \dot{d}\left(\frac{1}{(1-\xi^2)^{\frac{1}{2}}}\left\{1 - \frac{k}{\pi}(2+ka)^2\,\xi\log\left(\frac{1+\xi}{1-\xi}\right)\right\} - \frac{k}{2\pi}(2+ka)^2\,I(\xi)\right) \tag{B8}$$

where $\xi = x/d$ and I is defined by (B6).

Appendix C: Justification of the matching condition (69)

Here we detail the far-field contribution of the potential ϕ to the jet root region. The lower limit in (B5) is $\arccos\left(\frac{x}{d}\right)$. Let $\frac{x}{d} = 1 + \epsilon^2 x_j$ and $s = -\epsilon^2 x_j$, where $x_j < 0$ in the region of interest. We also have, for small $s \geq 0$, $\arccos(1-s) \approx \sqrt{2s}$.

So we let $S = \sqrt{2s}$ be the limit in the integral:

$$\int_{\arccos\left(\frac{x}{d}\right)}^{0} \log\left(\tan^2\left(\frac{\theta}{2}\right)\right)\mathrm{d}\theta = \int_S^0 \log\left(\frac{1-\cos\theta}{1+\cos\theta}\right)\mathrm{d}\theta. \tag{C9}$$

Since S is small, θ is small over the integration range, and we can approximate using the truncated Maclaurin series $\cos\theta = 1 - \frac{\theta^2}{2}$, thus we have

$$\int_S^0 \log\left(\frac{1-\cos\theta}{1+\cos\theta}\right)\mathrm{d}\theta = \int_S^0 \log\left(\frac{\theta^2}{4+\theta^2}\right)\mathrm{d}\theta \tag{C10}$$

We neglect θ^2 in the denominator in (C10) as it is small compared to 4. Hence

$$\int_S^0 \log\left(\frac{1-\cos\theta}{1+\cos\theta}\right)\mathrm{d}\theta \approx \int_S^0 \log\left(\frac{\theta^2}{4}\right)\mathrm{d}\theta = -\left(2S\log(S) - 2S - 2S\log(2)\right). \tag{C11}$$

In (C11) $2S\log(S)$ is non-singular, and is the dominant term as $S \to 0$. Since $S = O(\epsilon)$ the integral is $O(\epsilon\log(\epsilon))$.

Taking the factor multiplying this integral into account in (59) the leading order of this factor is $O(k)$. So for small k this term will never be present at leading order, leaving only the term corresponding to the impermeable solution.

The remaining part of this expression for ϕ in (59) is:

$$\sqrt{d^2 - x^2} = \sqrt{d^2 - (d + \epsilon^2 x_j)^2} \tag{C12}$$

$$= \epsilon \left(\sqrt{-2dx_j} + O(\epsilon^2) \right), \tag{C13}$$

valid for $x_j < 0$, with $d = O(1)$ we have the leading order to be $O(\epsilon)$. Thus our matching condition for ϕ_j at leading order is

$$\epsilon \left(\phi_j + \dot{d}x_j \right) = \epsilon \sqrt{-2dx_j}, \tag{C14}$$

$$\phi_j(x_j, 0, t) = \sqrt{-2dx_j} - \dot{d}x_j. \tag{C15}$$

Hence (69).

References

1. Dam DB, Le Clerc C (2004) Experimental study of the impact of an ink-jet printed droplet on a solid substrate. Phys Fluids 16(9):3403–3414. https://doi.org/10.1063/1.1773551
2. Hoath SD (ed) (2016) Fundamentals of inkjet printing: the science of inkjet and droplets. John Wiley & Sons, Hoboken
3. Martin GD, Hoath SD, Hutchings IM (2008) Inkjet printing-the physics of manipulating liquid jets and drops. J Phys 105:012001. https://doi.org/10.1088/1742-6596/105/1/012001
4. Mazur R, Ryżak M, Sochan A, Beczek M, Polakowski C, Przysucha B, Bieganowski A (2022) Soil deformation after one water-drop impact-the effect of texture and soil moisture content. Geoderma 417:115838
5. Zhang S, Hu X, Lourenço SD (2023) Modelling of water droplet dynamics on hydrophobic soils: a review. In: E3S Web of Conferences, vol 382, p 18005. EDP Sciences
6. Hicks PD, Crosby A, Hewitt D, Hennessy M, Herterich J, Moyles I (2012) Liquid interactions with porous media and the fate of toxic materials. European Study Group with Industry (ESGI) report
7. Lee J, Derome D, Carmeliet J (2016) Drop impact on natural porous stones. J Colloid Interface Sci 469:147–156
8. Srikar R, Gambaryan-Roisman T, Steffes C, Stephan P, Tropea C, Yarin AL (2009) Nanofiber coating of surfaces for intensification of drop or spray impact cooling. Int J Heat Mass Trans 52(25–26):5814–5826. https://doi.org/10.1016/j.ijheatmasstransfer.2009.07.021
9. Han D, Steckl AJ (2009) Superhydrophobic and oleophobic fibers by coaxial electrospinning. Langmuir 25(16):9454–9462. https://doi.org/10.1021/la900660v
10. Marston JO, Thoroddsen ST, Ng WK, Tan RBH (2010) Experimental study of liquid drop impact onto a powder surface. Powder Technol 203:223–236
11. Gilet T, Bourouiba L (2014) Rain-induced ejection of pathogens from leaves: revisiting the hypothesis of splash-on-film using high-speed visualization. The Society for Integrative and Comparative Biology
12. Gart S, Mates JE, Megaridis CM, Jung S (2015) Droplet impacting a cantilever: a leaf-raindrop system. Phys Rev Appl 3(4):044019
13. Maitra T, Antonini C, Tiwari MK, Mularczyk A, Imeri Z, Schoch P, Poulikakos D (2014) Supercooled water drops impacting superhydrophobic textures. Langmuir 30(36):10855–10861
14. Maitra T, Tiwari MK, Antonini C, Schoch P, Jung S, Eberle P, Poulikakos D (2014) On the nanoengineering of superhydrophobic and impalement resistant surface textures below the freezing temperature. Nano Letters 14(1):172–182
15. Tran T, Staat HJJ, Susarrey-Arce A, Foertsch TC, Houselt A, Gardeniers HJGE, Prosperetti A, Lohse D, Sun C (2023) Droplet impact on superheated micro-structured surfaces. Soft Matter 9:3272–3282. https://doi.org/10.1039/C3SM27643K
16. Tsai P, Veen RCA, Raa M, Lohse D (2010) How micropatterns and air pressure affect splashing on surfaces. Langmuir 26(20):16090–16095. https://doi.org/10.1021/la102330e
17. Raza MA, Swigchem J, Jansen HP, Zandvliet HJW, Poelsema B, Kooij ES (2014) Droplet impact on hydrophobic surfaces with hierarchical roughness. Surf Topogr Metrol Prop 2(3):035002. https://doi.org/10.1088/2051-672X/2/3/035002
18. Yarin AL (2006) Drop impact dynamics: sdplashing, spreading, receding, bouncing. Annu Rev Fluid Mech 38:159–192

19. Josserand C, Thoroddsen ST (2016) Drop impact on a solid surface. Annu Rev Fluid Mech 48:365–391
20. Wang X, Xu B, Guo S, Zhao Y, Chen Z (2023) Droplet impacting dynamics: recent progress and future aspects. Adv Colloid Interf Sci 7:102919
21. Wagner H (1932) Phenomena associated with impacts and sliding on liquid surfaces. Z Angew Math Mech 12(4):193–215
22. Wilson SK (1989) The mathematics of ship slamming. DPhil thesis, Oxford University
23. Howison SD, Ockendon JR, Wilson SK (1991) Incompressible water-entry problems at small deadrise angles. J Fluid Mech 222:215–230
24. Oliver JM (2002) Water entry and related problems. DPhil thesis, Oxford University
25. Howison SD, Ockendon JR, Oliver JM, Purvis R, Smith FT (2005) Droplet impact on a thin fluid layer. J Fluid Mech 542:1–23
26. Ellis AS, Smith FT, White AH (2011) Droplet impact onto a rough surface. Q J Mech Appl Math 64(2):107–139. https://doi.org/10.1093/qjmam/hbq026
27. Hicks PD (2022) Violent droplet impacts with non-flat surfaces. J Fluid Mech 939:31
28. Pegg M, Purvis R, Korobkin A (2018) Droplet impact onto an elastic plate: a new mechanism for splashing. J Fluid Mech 839:561–593
29. Khabakhpasheva T, Korobkin A (2020) Splashing of liquid droplet on a vibrating substrate. Phys Fluids 32(12):122109
30. Elliott J, Smith F (2017) Ice formation on a smooth or rough cold surface due to the impact of a supercooled water droplet. J Eng Math 102:35–64
31. Clarke A, Blake T, Carruthers K, Woodward A (2002) Spreading and imbibition of liquid droplets on porous surfaces. Langmuir 18(8):2980–2984
32. Reis NC Jr, Griffiths RF, Santos JM (2008) Parametric study of liquid droplets impinging on porous surfaces. Appl Math Model 32(3):341–361
33. Cooker MJ (2013) A theory for the impact of a wave breaking onto a permeable barrier with jet generation. J Eng Math 79:1–12
34. Moreton G (2022) Droplet impacts onto porous substrates: pre-and post-impact dynamics. PhD thesis, University of East Anglia
35. Hicks PD, Purvis R (2015) Gas-cushioned droplet impacts with a thin layer of porous media. J Eng Math 102:65–87
36. Oliver JM (2007) Second-order Wagner theory for two-dimensional water-entry problems at small deadrise angles. J Fluid Mech 572:59–85
37. Lamb H (1932) Hydrodynamics. Cambridge University Press, Cambridge
38. Negus MJ, Moore MR, Oliver JM, Cimpeanu R (2021) Droplet impact onto a spring-supported plate: analysis and simulations. J Eng Math 128:3